

Hydrodynamic alignment of microswimmers in pipes

Norihiro Oyama,¹ John Jairo Molina,² and Ryoichi Yamamoto^{2,3}

¹*Mathematics for Advanced Materials-OIL, AIST-Tohoku University, Sendai 980-8577, Japan*

²*Department of Chemical Engineering, Kyoto University, Kyoto 615-8510, Japan*

³*Institute of Industrial Science, The University of Tokyo, Tokyo 153-8505, Japan.*

(Dated: March 1, 2022)

We investigate the dynamics of model microswimmers under confinement, in cylindrical geometries, by means of three dimensional direct numerical calculations with fully resolved hydrodynamics. Such swimmers are known to show collective alignment in bulk, and we confirmed that similar alignment can be observed even in pipes, although the volume fraction dependency shows qualitative differences. By comparing the structural information, we investigated the cause of such differences. We found an order/disorder phase transition for a specific type of swimmers, as the size of the pipe becomes comparable to the size of the swimmers. Such dynamics are found not to depend on the geometry of confinement.

PACS numbers: 87.16.Uv, 78.20.Bh

I. INTRODUCTION

Self-propelled particles (SPPs) are attracting more and more interest as a representative example of out-of-equilibrium systems[1–12]. Examples of SPPs range from the microscopic scale, with algae and bacteria, to the macroscopic scale, which includes all animals, and recently, even artificial SPPs have been constructed, such as active Janus particles[13–16] or self-propelled droplets[17, 18]. Among them, microswimmers are of particular interest[12], since they are suited to well-controlled lab experiments[19], and have many potential applications, for example, as targeted drug delivery systems. It is known that nontrivial motion, like the collective alignment of the swimming direction or the dynamic clustering can be observed, even for systems where particles interact with each other only through hydrodynamic interactions and excluded volume effects[20–22]. Such collective motion is mainly due to the complicated hydrodynamic interactions, and cannot be predicted only from knowledge of the single particle dynamics. That these hydrodynamic interactions are strongly affected by the presence of confining walls is well known[23–25]. Experimentally, Das *et al.* reported that when a single Janus particle swims in the vicinity of a wall, it tends to swim along the wall[26]. Lushi *et al.* investigated the collective dynamics of a bacterial dispersion inside a circular confinement, and reported that the system spontaneously shows an anomalous double-vortex motion[19]. Regarding the theoretical or numerical studies with full hydrodynamics, while most of them have focused on the dynamics in bulk, several works have reported on the dynamics of microswimmers near walls or under confinement[19, 22, 26–33]. The dynamics under confinement is usually studied using flat parallel walls or cylindrical pipes. We would like to note that works with nonspherical swimmers[34] or chemically actuated swimmers[35] with confinements have been reported. Also, the dynamics of microswimmers in external field[36, 37] or with background flow[38, 39] have

also been investigated. In the present work, we focus on spherical swimmers which self-propel by utilizing only the hydrodynamic interactions between the ambient fluid, so-called “squirmers”[9, 40–42]. In this description of microswimmers, different types of swimming mechanisms can be expressed only by changing one parameter, which we refer to as the swimming parameter. As examples of the work using the same swimmer description as ours, Li and Ardekani have investigated the static structure between flat parallel walls and shown evidence for the accumulation of particles near the wall[28]. Zöttl and Stark have studied a similar system[29], but under extreme confinement, and observed a dense-dilute phase separation, which is not seen in bulk. Our previous work[22] has focused on the dynamic properties of a microswimmer dispersion confined between flat parallel walls with relatively large separations (compared to the size of the particles). In ref. [22], we observed a traveling wave-like collective motion for a specific range of swimming parameters and densities. Though such a motion would seem to be a consequence of confinement, we clarified that it can be understood as the manifestation of the pseudo-acoustic properties of the system, which is already observed in bulk. As shown here, even for the same confinement geometry, the dynamic behavior can be considerably different depending on the strength of the confinement (i.e., the wall separation). Therefore, how the dynamics changes under confinement is a very difficult question to answer.

Although we can find several works on the collective dynamics in bulk or between flat parallel walls, the many particle dynamics of swimmers in pipes has not been extensively studied so far. This is the focus of the present work. Intuitively, we can expect that for big enough pipes, the dynamics will be the same as for bulk systems. Therefore, we focus on the dynamics in pipes with diameters comparable to that of the particle, where we can expect nontrivial behaviors which are different from those in bulk. In fact, in the work by Zhu *et al.*, which deals with the single particle dynamics in a pipe, it is reported

that different dynamical modes can be observed depending on the swimming type and strength[27]. Taking into account the possibility that the size and the shape of the pipe affect the dynamic properties, in this work, we investigated the collective alignment effects, known as the polar order formation, varying the four main parameters, namely, the pipe size, the pipe shape, the volume fraction and the type of the swimmers. Regarding the polar order formation in many particle systems, the behavior in pipes is mostly the same as in bulk, if the pipe size is large enough. However, for a specified region of the parameter space, we observed clear wall effects, which we investigated by measuring the structural information of the dispersion. In addition, we observed the pipe size dependent order/disorder phase transition only for the parameters at which clustering behaviors have been reported in bulk and between flat walls[21, 22]. In this work, we also measured the bulk structural information and obtained indirect evidences which states that the clustering is important for the collective alignment for a specific range of parameters.

II. SIMULATIONS

A. The Squirmer Model

As the numerical model for microswimmers, we employed the squirmer model[40, 41]. In this model, the microswimmers are expressed by rigid particles with a prescribed flow field on their surface. The general squirmer model is expressed in the form of an infinite expansion, with components along the tangential, radial, and azimuthal directions. However, utilizing only the first two modes of the tangential field, following Eq. (1), already enables us to model different types of swimmers, namely pushers, pullers and the neutral swimmers.

$$\mathbf{u}^s(\theta) = B_1 \left(\sin \theta + \frac{\alpha}{2} \sin 2\theta \right) \hat{\boldsymbol{\theta}}, \quad (1)$$

where, \mathbf{u}^s denotes the surface flow field, $\hat{\mathbf{r}}$ is a unit vector directed from the center of the particle to a point on its surface, $\theta = \cos^{-1}(\hat{\mathbf{r}} \cdot \hat{\mathbf{e}})$ the polar angle between $\hat{\mathbf{r}}$ and the swimming direction $\hat{\mathbf{e}}$, and $\hat{\boldsymbol{\theta}}$ is the tangential unit vector at $\hat{\mathbf{r}}$. This simplified squirmer model has been widely used and is known to lead to a wide variety of nontrivial phenomena[6]. The coefficient of the first mode, B_1 , determines the swimming velocity of an isolated squirmer ($U_0 = 2/3B_1$), and that of the second mode, B_2 , determines the stresslet[42]. The ratio between the coefficients of the two modes, $\alpha = B_2/B_1$ in Eq. (1), determines the swimming type and strength. In the following, we call α the swimming parameter. Negative values of α represents pusher-type swimmers, which swim with an extensile flow field in the swimming direction, and positive values describe puller-type swimmers, which swim with a contractile flow. A value of $\alpha = 0$

stands for a neutral swimmer, which generates a potential flow field. In this model, the prescribed flow field is assumed to be an axisymmetric pure tangential one and the particle is rigid and spherical. These are the only assumptions employed to derive the model. Therefore, it is thought that this model can capture even the features of the artificial microswimmers like Janus particles even though it was originally intended to describe ciliary propulsion of micro-organisms.

B. Smoothed Profile Method (SPM)

In this work, we investigate the dynamics of squirmer particles swimming in a viscous fluid. For this, we must solve the combined fluid-solid problem. The Newton-Euler equations of motion govern the particle trajectories:

$$\begin{aligned} \dot{\mathbf{R}}_i &= \mathbf{V}_i & \dot{\mathbf{Q}}_i &= \text{skew}(\boldsymbol{\Omega}_i) \cdot \mathbf{Q}_i \\ M_p \dot{\mathbf{V}}_i &= \mathbf{F}_i^H + \mathbf{F}_i^C & \mathbf{I}_p \cdot \dot{\boldsymbol{\Omega}}_i &= \mathbf{N}_i^H \end{aligned} \quad (2)$$

where the subscript i means the particle index, \mathbf{R} the position vector, \mathbf{Q} the orientation matrix, $\text{skew}(\boldsymbol{\Omega})$ the skew symmetric matrix of the angular velocity $\boldsymbol{\Omega}$, and \mathbf{F}^H and \mathbf{N}^H the hydrodynamic force and torque though which the particle dynamics is coupled with the flow field. The interaction between particles, \mathbf{F}^C , is also considered to prevent overlapping of the particles by employing a repulsive Lennard-Jones type potential, or the Weeks-Chandler-Andersen potential. As the powers for the potential, we adopted 36-18:

$$\mathbf{F}_i^C = \sum_j \mathbf{F}_{ij}, \mathbf{F}_{ij} = -\nabla_i U(r_{ij}), \quad (3)$$

$$U(r_{ij}) = \begin{cases} 4\epsilon \left[\left(\frac{\sigma}{r_{ij}} \right)^{36} - \left(\frac{\sigma}{r_{ij}} \right)^{18} \right] + \epsilon & (r_{ij} \leq r_C) \\ 0 & (r_{ij} \geq r_C) \end{cases} \quad (4)$$

where, $r_C = 2^{1/18}\sigma$ is the cutoff length. ϵ gives the strength of the potential and is the unit of energy in the system. Due to the steep nature of the potential, the value of ϵ affect only weakly to the system dynamics. The time evolution of the fluid flow field \mathbf{u}_f is described by the Navier-Stokes equation with the incompressible condition:

$$\nabla \cdot \mathbf{u}_f = 0 \quad (5)$$

$$\rho_f (\partial_t + \mathbf{u}_f \cdot \nabla) \mathbf{u}_f = \nabla \cdot \boldsymbol{\sigma}_f \quad (6)$$

$$\boldsymbol{\sigma}_f = -p\mathbf{I} + \eta \left\{ \nabla \mathbf{u}_f + (\nabla \mathbf{u}_f)^t \right\} \quad (7)$$

where $\boldsymbol{\sigma}_f$ is the stress tensor, ρ_f the mass density of the host fluid and η the shear viscosity. In order to solve these simultaneous equations efficiently, we employed the Smoothed Profile Method (SPM). In the SPM, we don't treat the sharp boundary between the solid and fluid

phases explicitly. Instead, a diffuse interface with thickness of ξ is introduced, and the phase boundaries are expressed by using a continuous order parameter ϕ , which takes the value of one in the solid domain, zero in the fluid domain, and intermediate values within the diffuse interface region. Employing this method, all the physical quantities can be expressed in terms of continuous fields defined over the whole computational domain. The total velocity field \mathbf{u} which includes both particle and fluid velocity information can be expressed like:

$$\mathbf{u} = (1 - \phi) \mathbf{u}_f + \phi \mathbf{u}_p, \quad (8)$$

$$\phi \mathbf{u}_p = \sum_i \phi_i [\mathbf{V}_i + \boldsymbol{\Omega}_i \times \mathbf{R}_i]$$

where, $(1 - \phi) \mathbf{u}_f$ and $\phi \mathbf{u}_p$ are the contribution of the fluid flow field and the particle motion to the total velocity field. And now, the time evolution of the total velocity field \mathbf{u} is governed by a modified incompressible Navier-Stokes equation:

$$\rho_f (\partial_t + \mathbf{u} \cdot \nabla) \mathbf{u} = \nabla \cdot \boldsymbol{\sigma}_f + \rho_f (\phi \mathbf{f}_p + \mathbf{f}_{sq}), \quad (9)$$

$$\nabla \cdot \mathbf{u} = 0, \quad (10)$$

where $\phi \mathbf{f}_p$ is the body force guaranteeing the rigidity condition of particles and \mathbf{f}_{sq} the force needed to maintain the squirming motion. By doing this, the calculation cost can be reduced by orders of magnitude. See refs.[43–46] for more detailed information about this method.

In this work, the dynamics of swimmers in pipes are considered. For this, we have to model solid walls numerically. Within the SPM scheme, the walls can be expressed by assemblies of particles which are pinned and not allowed to translate or rotate. By this, the stick boundary at the wall surface is guaranteed. The wall particles are placed uniformly and have the same diameter as the swimmer particles. Because we consider various shapes and sizes of pipes, the number of particles composing the walls varies depending on the pipe. We confirmed that the roughness due to the wall representation as a collection of discrete particles has only a weak effect on the particle dynamics. All the quantities are non-dimensionalized in terms of the grid spacing Δ , the viscosity η and the density of the fluid ρ_f in our calculations and these values are set to be unity. No noise is included in any of the calculations in this work (the limit of the infinite Peclet number), unless stated otherwise.

C. System Parameters

Using the calculation method presented above, we conducted three-dimensional direct numerical simulations (DNS) of microswimmer dispersions confined in pipes. The diameter σ and interface thickness ξ of particles are set to be $\sigma = 6\Delta$ and $\xi = 2\Delta$ respectively, where Δ stands for the grid spacing. The excluded volume effect between particles (both wall-particle and particle-particle) is implemented by \mathbf{F}^C in Eq. (2),(3). Regarding

the parameters in Eq. (1), we set $B_1 = 0.25$ for all the calculations and varied α to study the α dependency of the dynamics. This value of B_1 gives a particle Reynolds number of one for an isolated swimmer (as presented above, only the value of B_1 determines the steady state velocity). The symmetry axis of the pipe is defined to be parallel to the y axis. In what follows, we refer to the confinement with a circular cross section as a pipe, and the one with a rectangular cross section as a duct. Regardless of the size or shape of confinement, the length of the pipe L is set to be $L = 128\Delta \approx 20\sigma$ and the periodic boundary condition is set in this direction (in other directions, the system is enclosed by the confinement, and the system size in those directions depends on the confinements). Unless stated otherwise, thermal fluctuations are ignored throughout this paper. We will consider the pipe with diameter $D = 8\sigma$ to be our reference confinement system, where D is defined as the diameter of the pipe containing the free space available to the particle. In this article, first we present the dynamics of this reference system, and then those obtained for different pipe sizes. For the definition of the particle volume fraction we used:

$$\varphi = \frac{N_p V_p}{V_M}, \quad (11)$$

where $V_p = \frac{1}{6}\pi\sigma^3$ is the volume of one particle and V_M the volume in which particle centers can move freely:

$$V_M = \frac{\pi}{4} L D^2. \quad (12)$$

III. RESULTS & DISCUSSIONS

A. Single-particle Dynamics in a Pipe

The single-particle dynamics in a pipe has been studied by Zhu *et al.*, who reported that distinct dynamical modes are observed depending on the swimming parameter α [27]. In order to confirm the qualitative agreement within our calculation scheme, we performed calculations with one particle for various values of α . As mentioned above, in this section, we consider only a pipe with diameter $D = 8\sigma$, the reference system. After a sufficiently long time, all the cases achieve steady states. Typical trajectories of the steady states are shown in Fig. (1). Here, the result of the cases with $\alpha = 0, \pm 1$ are shown. The dynamical mode at the steady state depends mostly on the sign of α : a pusher gets trapped in an orbit and shows constant rotation at a fixed y position, while a puller shows rectilinear translation along the pipe axis at a constant distance from the wall. A swimmer with $|\alpha| \leq 0.4$, including a neutral swimmer, achieves the combined dynamics of the two modes: spiral motion along the pipe axis (rotation + translation). The pitch of the spiral depends on the value of $|\alpha|$ and decreases (increases) with

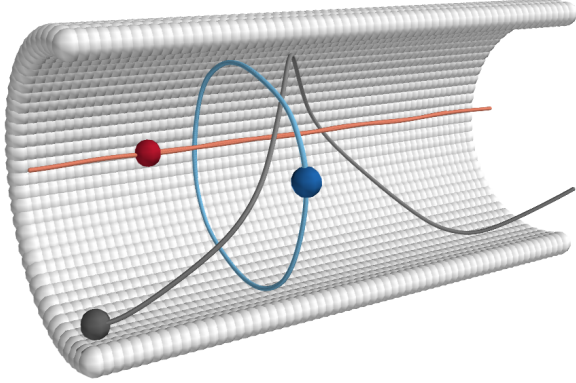


FIG. 1: Typical trajectories of the three different dynamical modes. (a) Pusher's rotational orbit ($\alpha = -1$; represented by blue) (b) Neutral swimmer's spiral trajectory ($\alpha = 0$; represented by gray) (c) Puller's rectilinear path ($\alpha = 1$; represented by red). Note that these three trajectories are obtained using the same initial position and orientation. Only the trajectories in steady states are shown. White particles represent the particles composing the pipe. To facilitate the visualization, only half of the pipe-particles are drawn.

the increase of $|\alpha|$ for the case of a pusher (puller). And eventually, at around $|\alpha| = 0.4$, the dynamical mode changes. These results are consistent with the results in ref.[27]; although the trajectories of the pushers are not analyzed in detail in ref.[27].

As shown here, the single-particle dynamics are affected by the confinement. The intriguing thing is that the dynamical mode depends on the swimming parameter α . Regarding the bulk collective properties, it is known that such a swimming parameter dependence exists as well. For example, the polar order P (Eq. (13)), often used to measure the degree of collective alignment, strongly depends on α .

$$P = \left\langle \frac{1}{N_p} \left| \sum_i \hat{e}_i \right| \right\rangle, \quad (13)$$

where, N_p stands for the number of particles in the system and \hat{e}_i the unit swimming direction vector of particle i . This quantitative measure of the degree of order, P , takes a value of one when the system is completely aligned, and $P \approx P_0 = 1/\sqrt{N_p}$ when the system is completely isotropic. The value of the polar order P decreases as the absolute value of α increases. Though the dynamical mode transition of the single swimmer motion in pipe occurs at the same absolute value of α , it is known that the bulk polar order P is asymmetric with respect to α : the order is broken faster for pushers than for pullers with increasing $|\alpha|$ [20–22].

B. Many Particle Dynamics in a Pipe

We next performed calculations for many particle systems in a pipe of diameter $D = 8\sigma$. The polar order P is a function of both the swimming parameter α , and the volume fraction of the particles φ . First of all, let us recapitulate the behaviors in bulk systems[47]. If we measure the polar order as a function of the swimming parameter α at a certain value of the volume fraction, the polar order P decreases with the increase in the absolute value of α , as stated above. This tendency is asymmetry with respect to positive and negative values of swimming parameter α : with negative values (pushers), showing a faster decay. If we regard the order parameter P as a function of the particle volume fraction φ for a certain value of the swimming parameter α , the behavior is most easily understood in terms of the deviations from the volume fraction dependence for neutral swimmers. This reference system ($\alpha = 0$) shows two regimes: for $\varphi \leq 0.4$, the values are constant; for $\varphi \geq 0.4$ there is an abrupt drop in the order parameter to that of a disordered state $P \approx P_0$. A similar behavior is observed for pushers (negative values of the swimming parameter α). At small volume fractions, they show only a weak decrease with increasing volume fraction, and then exhibit an abrupt drop at a critical volume fraction φ_c . Pushers show a decrease both in the degree of ordering and the value of φ_c . Pullers, on the other hand, show a decrease only in the degree of ordering, and systems of intermediate pullers ($\alpha = 0.5$, for example) even maintain the order at very high volume fractions, where all other systems show $P \approx P_0$. Specifically, we stress that in bulk, the system with $\alpha = 1$ shows a nonzero value of the polar order P up to very high volume fractions.

We conducted simulations over a wide range of combinations of the swimming parameter α and the volume fraction ϕ in the pipe. From the particle trajectories obtained from these simulations, we then calculated the polar order parameter along the y direction (the direction of the pipe elongation),

$$P_y = \left\langle \frac{1}{N_p} \left| \sum_i e_i^y \right| \right\rangle, \quad (14)$$

where e_i^y is the y -component of the swimming direction \hat{e} of particle i and the angular brackets denote a time average. In Fig. 2, the values of the in-pipe polar order P_y are shown as a function of α . Here, the values of the polar order parameter P in bulk are also shown using a lighter-colored line. The volume fraction is $\varphi \approx 0.25$ for both cases ($N_p = 500$ in the pipe, $N_p = 550$ in bulk). In Fig. 2, we see a good match between results in bulk and those in pipe over a wide range of α . However, for $0.5 < \alpha \leq 1.5$, we see clear differences. In pipes, over this α range, the values of P_y are reduced compared to the bulk results, with the gap increasing with an increase in the absolute value of α . Finally, at $\alpha \simeq 0.9$, the dynamics show a

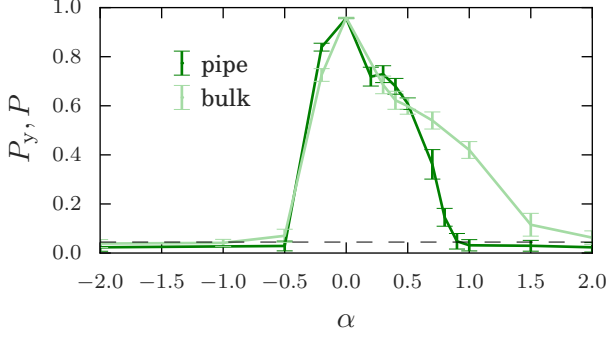


FIG. 2: The polar order parameter P_y in a pipe with diameter 8σ as a function of the swimming parameter α . The polar order P in bulk systems is also shown as a light-colored line. The volume fraction is $\varphi \approx 0.25$ in both cases. The dashed line stands for the value of P_0 .

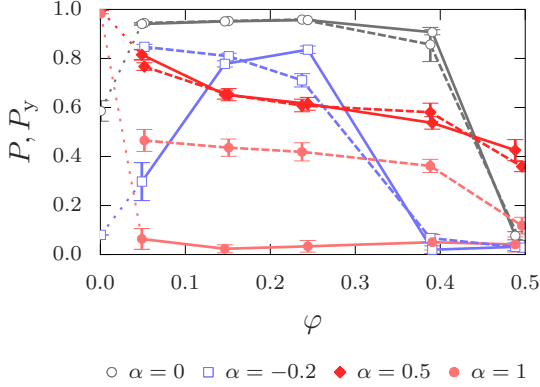


FIG. 3: The polar order parameter P_y in a pipe with diameter 8σ as a function of volume fraction φ and swimming parameter α . The polar order P in bulk systems is also shown using dashed lines. The dotted lines connect the results from multi-particle systems and those from single-particle systems in pipes.

qualitatively different behavior: in the pipe, $P_y = P_0$ which means the order is completely lost.

In Fig. 3, detailed results representing the volume fraction dependency are shown for four different values of the swimming parameter α , which exhibit qualitatively different behavior, $\alpha = -0.2, 0, 0.5, 1$. For the volume fraction, we consider five different values in the range of $0.05 \leq \varphi \leq 0.5$ (corresponding to $100 \leq N_p \leq 1150$). As before, the bulk results are shown as dashed lines in Fig. 3. Although the results in the pipe are qualitatively the same as those in bulk for some of the cases, several differences can be perceived. In the case with $\alpha = -0.2$, the value of P at the smallest volume fraction ($\varphi \approx 0.05$) shows an obvious reduction in the pipe compared to the

bulk. In addition, for this case ($\alpha = -0.2$), we observe a rise in P_y at intermediate volume fraction ($\varphi \approx 0.25$). In the case with $\alpha = 1$, we see no polar order ($P_y \simeq 0$) at any of the volume fractions considered. Lastly, we note that in the cases of $\alpha = 0, 0.5$ we observed a very good agreement between the results in bulk and those in the pipe over the whole range of volume fractions. We also show the value of the polar order P for the single-particle system in the pipe as the data for the infinite dilution systems with dotted line (though it leads to the volume fraction of $\varphi \approx 0.0005$). Note that the value of P for a single neutral swimmer depends on the initial orientation: if the initial orientation is parallel to the pipe axis, it shows a wave-like trajectory and the value of P is not constant. Here, we show the value for the case with a spiral motion where P is almost constant with time. Though we can smoothly extrapolate the missing data in the range below $\varphi = 0.05$ for the cases with $\alpha = -0.2, 0.5$, we see clear jumps for $\alpha = 0, 1$. Because the relaxation time to reach the steady state becomes very long as the volume fraction becomes small in the pipe, it is very difficult to investigate what is happening at such dilute systems. Especially, the clarification of the onset of jumps of the polar order P for the cases with $\alpha = 0, 1$, or the transition from the single particle motion to the collective motion, still remains an open question.

In order to understand these differences from the view point of the structures inside the pipe, we measured the following two functions, the local density $\rho(r_c)$ and the local polar order along the y -axis $p_y(r_c)$. These are defined as a function of the perpendicular distance r_c from the symmetry axis of the pipe:

$$\rho(r_c) = \left\langle \frac{N_c(r_c)}{2\rho_0\pi r_c L \Delta r_c} \right\rangle, \quad (15)$$

$$p_y(r_c) = \left\langle \frac{1}{N_c(r_c)} \left| \sum_{i \in \text{bin}} e_i^y \right| \right\rangle, \quad (16)$$

where N_c is the number of particles at a distance r_c from the pipe axis, $\rho_0 = \frac{N_p}{V_M}$ the average number density of the whole system, Δr_c the width of the cylindrical bins, and the summation in Eq. (16) is taken over all the particles in a given bin. The local density of the shell matches the overall average value when $\rho(r_c) = 1$. The results are shown in Fig. 4 for the same values of α shown in Fig. 3. From this figure, we can explain the differences seen in Fig. 3. In the case of $\alpha = -0.2$, when the volume fraction is small ($\varphi = 0.05$, (a)), particles show a strong tendency to accumulate in the vicinity of the wall and almost no particles are observed within the central region ($r_c \simeq 0$). Such a wall accumulation effect has been reported for active systems in general[48, 49], and several works on squirmers have also shown this behavior[22, 28]. At the same time, we can see that the local polar order is reduced in the vicinity of the wall. In other words, the pipe can be divided into two distinct regions from the view point of p_y : an inner region where the local order has a value similar to that of the corresponding bulk dis-

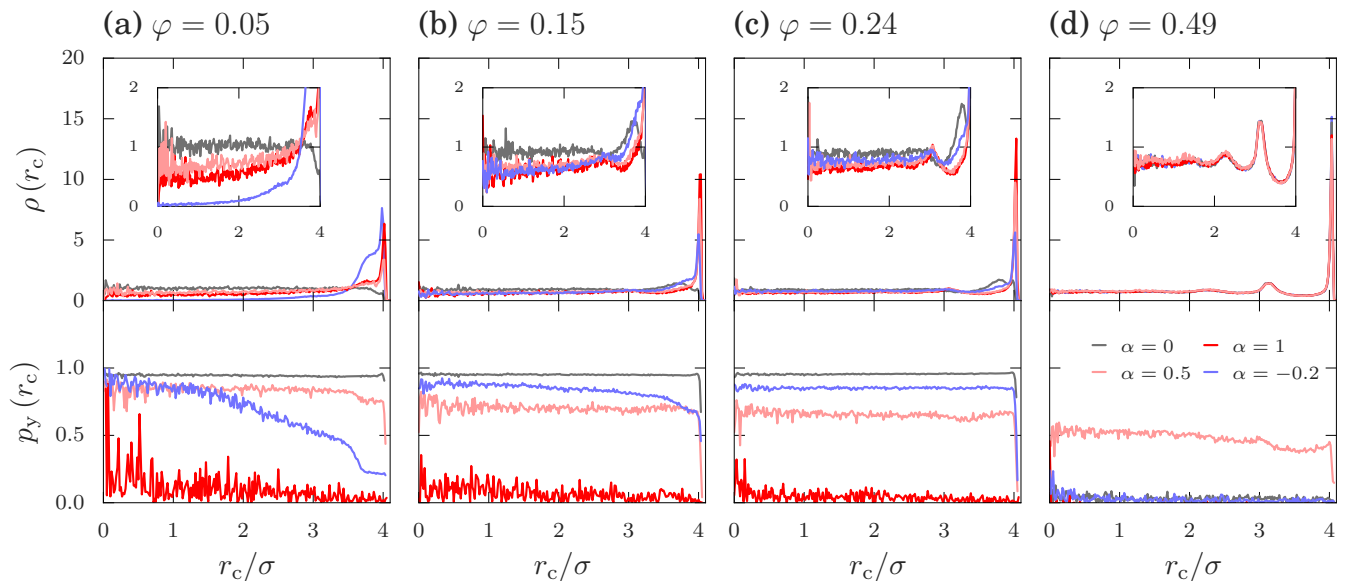


FIG. 4: The single-body density distribution ρ and the local polar order p_y for various combinations of φ and α . Insets show the images magnified in the y direction. The horizontal axis represents the distance from the pipe axis normalized by the particle diameter.

persion, and an outer region (near to the walls) where the order is reduced. In the following, we specify the characteristic size of this outer region by l_c , the distance from the wall to the point where the inner region starts. Because, in the case with $\alpha = -0.2$ and $\varphi = 0.05$, most particles accumulate in this outer region, where the order is reduced, the overall polar order is smaller than that in bulk. Then, as φ is increased, the particles will become more uniformly distributed, and l_c is reduced. At the same time, due to the wall accumulation effect, the effective volume fraction in the inner region is smaller than the global volume fraction. Taking into account the fact that the polar order increases with decreasing volume fraction, this reduction in the volume fraction leads to a higher local polar order at the inner region, compared to the bulk value at the same global volume fraction. As a result of these two effects, namely, the decrease in l_c and the increase of the local order due to the diluteness at the center, at $\varphi = 0.24$, the value of P_y is even larger than that in bulk for the case with $\alpha = -0.2$. In the case of other values of the swimming parameter ($\alpha = 0, 0.5$), such an overshoot is not observed. This is because for $\alpha = 0, 0.5$, the volume fraction dependency of the polar order is so small that the order is determined only by the value of l_c . For $\alpha = 1$, the value of l_c becomes very large and we don't see any ordering throughout the pipe, although the system with $\alpha = 1$ does show a nonzero value for polar order parameter P in bulk. In the limit when the diameter of the pipe goes to infinity, we expect the dynamics should converge to that observed in bulk. Therefore, we should see a qualitative transition at a critical diameter. This will be investigated in more detail in

Sec. III. C.. We also note that the behavior of ρ for $\alpha = 1$ is very similar to that of $\alpha = 0.5$ at all volume fractions, although the order formation tendencies are completely different. At the highest volume fraction $\varphi = 0.49$, because of the screening of the hydrodynamic interactions, the excluded volume effects become dominant in determining the structure. Consequently, the structure is the same for all values of α . However, it is interesting to note that only in the case of $\alpha = 0.5$, do we observe a nonzero value of P_y .

We have clarified that in many particle systems, the wall effects can be characterized by the accumulation of particles over a distance of l_c close to the walls. These can lead to both enhancement and inhibition of the ordering, depending on the degree of accumulation and the size of l_c . While for some cases we do observe a rectification effect due to the existence of walls, the origin for such effects seems to have nothing to do with the causes responsible for the single particle trajectories presented above.

C. Pipe size dependency

Here, we show results for the pipe diameter dependence of the dynamics. First, we present the results for the single-particle systems in a pipe with a “small” diameter. We present the results for a pipe with $D = 3\sigma$ as a reference system for the small pipe. For the single-particle systems, we have observed the same qualitative results as those for $D = 8\sigma$ (which we refer to as the “big” pipe). The only difference that can be seen is the

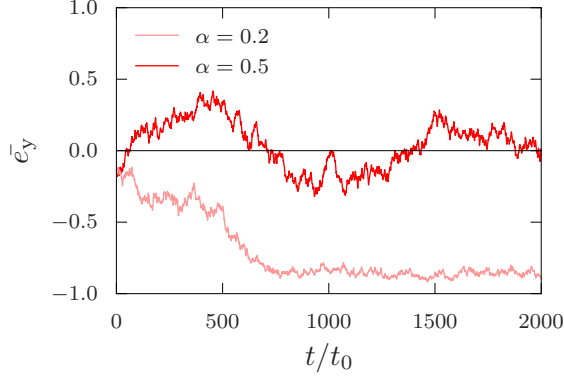


FIG. 5: The time evolution of the temporal order \bar{e}^y for systems with $\alpha = 0.2, 0.5$ in the small pipe with $D = 3\sigma$ at $\varphi = 0.28$. The horizontal axis gives the time normalized by $t_0 = \sigma/U_0$, where $U_0 = \frac{2}{3}B_1$ is the steady state velocity of an isolated swimmer. The vertical axis represents the value of temporal order.

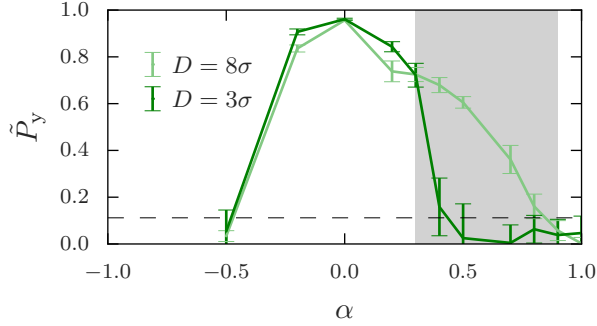


FIG. 6: The dependency on α of the polar order \tilde{P}_y in pipes. The dark lines are for the pipe with $D = 3\sigma$, while the light lines are for $D = 8\sigma$. The volume fraction is $\varphi \approx 0.25$ for both cases. The shaded region represents the region where the anomalous behavior was reported in ref.[22, 47].

value of α at which the dynamic mode transition occurs. Interestingly, such a change in the threshold is only seen for a pusher: for the small pipe, the threshold is around $\alpha = -2$. For a puller, the threshold is the same as the one in the pipe with $D = 8\sigma$ and it is $\alpha = 0.4$. Such asymmetric dependency on the swimming parameter α of the dynamics is also seen in the polar order parameter P (or P_y) as a function of α , as shown in Fig. 2. To conclude, the single-particle motion does not depend on the pipe size qualitatively.

Next, we investigated the polar order of many particle systems in the small pipe. In the small pipe, over a specific range of parameters, the value of the polar order doesn't show a stable nonzero value. In Fig. 5, the time evolution of the temporal order \bar{e}^y , defined in Eq. (17), is given for two cases to illustrate both the steady and

unsteady behaviors.

$$\bar{e}^y = \frac{1}{N_p} \sum_i^{N_p} e_i^y. \quad (17)$$

Both results are for a system with $D = 3\sigma$ and $\varphi = 0.28$ ($N_p = 80$). The steady results are for $\alpha = 0.2$, the unsteady one for $\alpha = 0.5$. As seen here, in the unsteady system, even the sign of \bar{e}^y , which represents the direction of motion, changes in time; while in the systems with stable order, such change is never observed. This change of direction shows the absence of any long-time persistent order in the pipe. In order to evaluate such direction-flipping behavior, we define an alternative in-pipe polar order parameter that can also indicate the persistence of the motion:

$$\tilde{P}_y = \left| \left\langle \frac{1}{N_p} \sum_i^{N_p} e_i^y \right\rangle \right|. \quad (18)$$

Only the order of taking the average and the absolute value is changed with respect to the standard definition of the polar order P_y , Eq. (14). For the cases in which the direction doesn't change, the values P_y and \tilde{P}_y are essentially the same. We measured \tilde{P}_y in the small pipe for various values of α and compared the results with those obtained for the big pipe. The results are shown in Fig. 6 at a volume fraction of $\varphi \approx 0.25$. We observe a remarkable differences over the range $0.4 \leq \alpha \leq 0.7$. In the small pipe for this range of values of α , \bar{e}^y has no steady state value and changes directions, as described above. Actually, for such systems, the values of \tilde{P}_y are around P_0 , which means that the system has no order. We consider this collapse of the order as an order/disorder phase transition. The gray-shaded region in Fig. 6 indicates the range of α at which anomalous behaviors were reported in preceding studies[22, 47]. In ref.[22], the dynamics of swimmer dispersions between flat parallel walls was studied. It was reported that, over this gray-shaded range of α , particles form big clusters, which exhibit a traveling wave-like motion, bouncing back and forth between walls. Interestingly, the shaded area corresponds very well to the region over which we observe the pipe-size dependent order/disorder transition in the present work. We refer to pullers in these regions as “intermediate” pullers. For α values other than those of intermediate pullers, the results are roughly the same between $D = 8\sigma$ and $D = 3\sigma$. We note that we have confirmed that the same qualitative results are obtained for different values of φ , at least over the range we have considered ($0.05 \leq \varphi \leq 0.25$). We would also like to stress that in bulk, we have observed a similar order/disorder phase transition when we change the volume fraction[20, 47]: when the volume fraction becomes very high, none of the swimmers except intermediate pullers are able to maintain the polar order. In contrast, in pipes, only intermediate pullers lose their polar order when the size of the pipe becomes small.

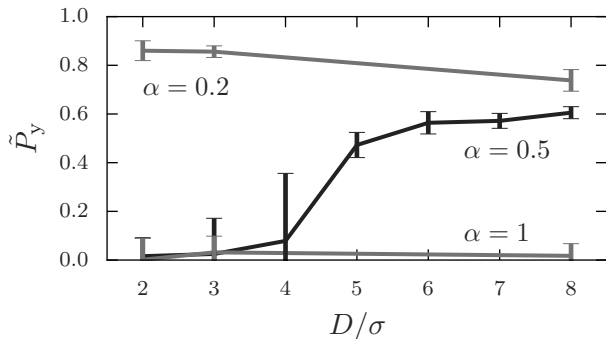


FIG. 7: The pipe diameter dependency of the in-pipe polar order \tilde{P}_y . The horizontal axis represents the pipe diameter D normalized by the particle diameter. The volume fraction is $\varphi \approx 0.25$ for all cases.

We have also investigated the detailed size dependency of the polar order for intermediate pullers. In Fig. 7, the values of the polar order \tilde{P}_y are shown as a function of the pipe diameter. Here, the results are shown not only for intermediate pullers $\alpha = 0.5$, but also for weak and strong pullers $\alpha = 0.2, 1$, which don't show the phase transition. The volume fraction is $\varphi \approx 0.25$ for all cases ($40 \leq N_p \leq 500$, depending on the size of the pipe). We see an abrupt drop of \tilde{P}_y at the critical diameter $D_c = 4\sigma$, though at higher D , the values are constant. In systems with $D \leq 4\sigma$, the value of \tilde{P}_y does not achieve the steady state, similar to the situations seen in Fig. 6. In other words, in such small pipes, intermediate pullers cannot maintain the polar order anymore, though temporally they can exhibit order. We believe this sensitivity to the pipe size suggests that intermediate pullers need clusters bigger than a characteristic size D_c to stabilize the polar order.

In order to specify the size of the cluster in bulk, we performed bulk simulations and measured the generalized radial distribution functions $g_n(r)$ [21],

$$g_n(r) = \left\langle \frac{1}{4\pi r^2 \Delta r} \frac{1}{\rho_0 (N_p - 1)} \sum_{i=1}^{N_p} \sum_{j \in \text{bin}} P_n(\cos \theta_{ij}) \right\rangle, \quad (19)$$

where r represents the distance from a reference particle i to a second particle j , $\theta_{ij} = \cos^{-1}(\hat{e}_i \cdot \hat{e}_j)$ the relative angle between the swimming directions of both particles, and P_n is the n -th degree Legendre polynomial. The zeroth-order function $g_0(r)$ is the standard radial distribution function, and the first-order function $g_1(r)$ represents the local degree of orientational order. In the limit when $r \rightarrow \infty$, we expect $g_0(r \rightarrow \infty) \sim 1$ and $g_1(r \rightarrow \infty) \sim P^2$. Therefore, we can define the excess local order $\delta P(r) = \sqrt{g_1} - P$, in such a way that it will converge to zero in the limit of $r \rightarrow \infty$. The bulk system considered here has a cubic domain with a linear dimension

of $128\Delta \approx 20\sigma$. Periodic boundary conditions are used in all directions, and the particles have the same diameter and interface thickness as in the simulations discussed above. The volume fraction is tuned by changing the number of particles, $1000 \leq N_p \leq 9000$. The calculated results for $g_0(r)$, $g_1(r)$ and $\delta P(r)$ are shown in Fig. 8, for $\varphi = 0.05, 0.16, 0.24, 0.49$ and $\alpha = -0.2, 0, 0.5, 1$, corresponding to the confined systems in Fig. 4. In addition, results for $g_0(r)$ for passive colloidal systems are shown to aid in comparison. For these passive systems, the temperature is set so that $k_B T = \epsilon$, where $\epsilon = \frac{\Delta \eta^2}{\rho_f}$ is the energy unit in our system. The exact value of the temperature does not affect the radial distribution function, provided that it is small enough.

To begin the analysis of the structure, we discuss the behavior of $g_0(r)$ for the reference system of passive colloids. At the smallest volume fraction ($\varphi = 0.05$), it shows only a small first peak around $r = \sigma$, and quickly decays, converging to one around $r = 1.5\sigma$. The intensity of this first peak becomes larger as the volume fraction increases. At a volume fraction of $\varphi = 0.16$, we observe a shallow undershoot after the first peak. The correlation length becomes longer and the value converges to one at around $r = 2\sigma$. At $\varphi = 0.24$, it starts to show a second peak at a position $r \gtrsim 2\sigma$, though the intensity is very small. Finally, at $\varphi = 0.49$, the system is in a mixed state of ordered and disordered phases[50], and shows four clearly distinguishable peaks (see inset magnified figures in Fig. 8(d)).

Now, we would like to present the results for the active systems. In the case of neutral swimmers ($\alpha = 0$), for all the volume fractions but the highest one, the first peak is smaller or shifted to larger distances compared to the passive system. In addition, the first peak doesn't even appear at the lowest volume fraction, $\varphi = 0.05$. These behaviors may indicate that there is an effective repulsive interaction between particles caused by the flow field. Due to this repelling flow field, neutral swimmers tend to get distributed uniformly. Similar effects can be seen in the pipe, as shown in Fig. 4 where neutrals swimmers show a much more uniform distribution compared to the other types of swimmers. The correlations beyond the first peak follow closely those of the passive system, while other swimmers show longer ranged correlations. This tendency may reflect the fact that the flow field around a neutral swimmer (decaying as r^{-3}) is more localized, because of the lack of the force dipole term (decaying as r^{-2} ; the second term in Eq. 1). Regarding $g_1(r)$, the qualitative behavior follows that of $g_0(r)$. We note that the neutral swimmers exhibit a unique behavior around $r = 2\sigma$, where $\delta P(r)$ shows negative values for intermediate values of $\varphi = 0.16, 0.24$.

In the case of $\alpha = -0.2$ and 1 , the results are quite similar for all the volume fractions, although the peak heights show slight differences. In these cases, the particles seem to show effective attraction due to the flow field, resulting in higher peaks for $g_0(r)$. As before, $g_1(r)$ follows the qualitative behavior seen in $g_0(r)$. Besides the

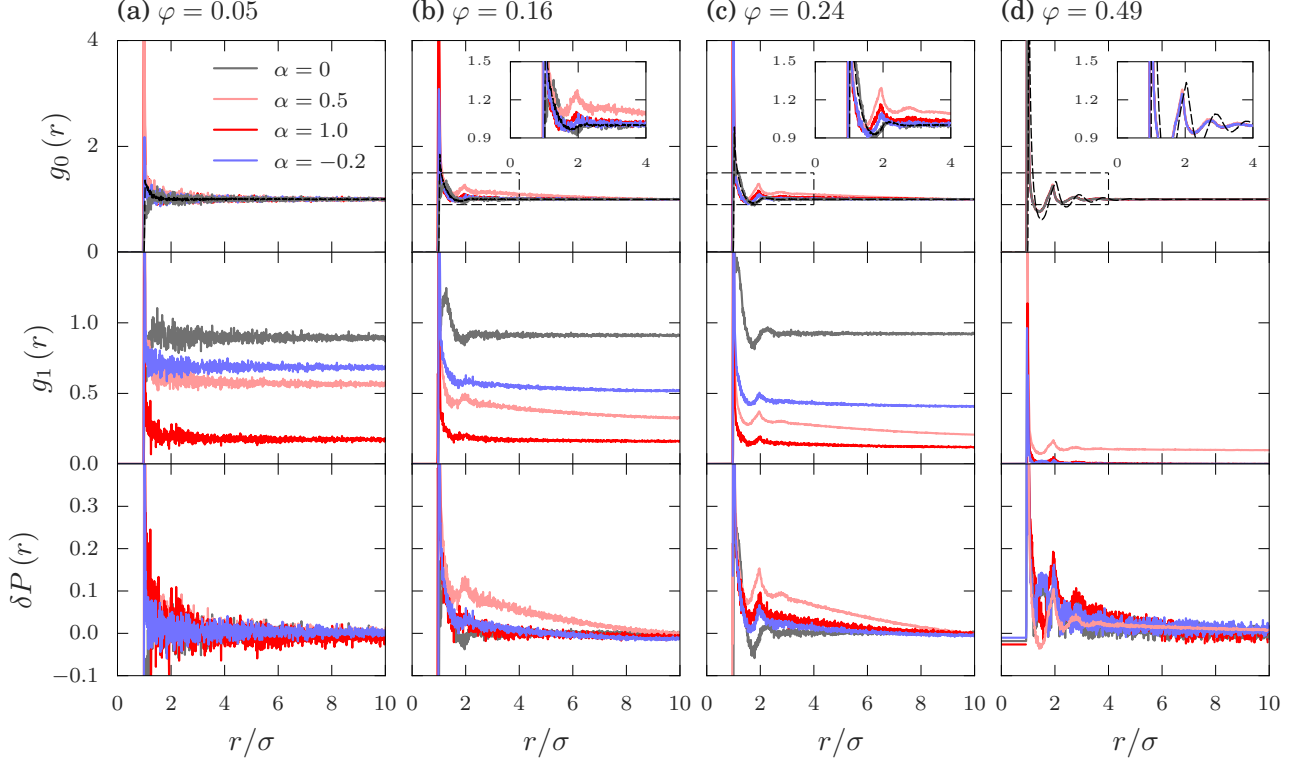


FIG. 8: The generalized radial distribution functions g_0 , g_1 and the local deviation of the order δP with respect to bulk values for various combinations of the volume fraction φ and the swimming parameter α . Insets show the images magnified in both x and y directions. The horizontal axis represents the distance from the reference particle normalized by the particle diameter.

higher peaks, the correlation length is longer than that seen for neutral swimmers. However, the bulk values are reached by $r \approx 6\sigma$ in all cases.

In the case with $\alpha = 0.5$, or intermediate pullers, many unique behaviors can be observed. First of all, $g_0(r)$ shows much more outstanding peaks than in any of the other cases. At $\varphi = 0.16$, only intermediate pullers show a definite second peak, and at $\varphi = 0.24$, the second peak is much higher than in the other systems, and a third peak even appears. A similar peak behavior can be observed also in the plot of $\delta P(r)$. In addition, we see a very long tail, which is not seen in the other cases. All these unique behaviors for intermediate pullers can be understood as indirect evidence for their already known dynamic clustering tendency[21, 22]. The high peaks reflect the clustering behavior, and the long tail in $g_1(r)$ shows the highly localized ordering. The nonzero order at high volume fractions helps explain how intermediate pullers can swim collectively, even under such extreme conditions. We note that the critical diameter of the pipe D_c is bigger than any of the peaks detected here.

At the highest volume fraction, $\varphi = 0.49$, the shapes of $g_0(r)$ are the same for all α , while only the passive system shows a different shape. Regarding the neutral swimmer

systems, $\alpha = 0$, this is notable because this system shows quite similar shapes at all the other volume fractions. The shape difference of $g_0(r)$ between the passive and active systems at $\varphi = 0.49$ may be due to the phase transition of the passive system. For passive hard-spheres, the volume fraction in the range $0.5 < \varphi < 0.55$ is known as the transient state of the ordered state and the disordered state[50]. In the passive system at $\varphi = 0.49$, shown in Fig. 8, such an ordered state seems to appear, while the active systems are still completely in the fluid phase. At this volume fraction, because the excluded volume effect is the dominant factor to determine the structure, rather than the flow field, all the active systems show the same shape for g_0 . In summary, although we could not obtain a direct connection between the bulk structural information and the in-pipe order/disorder phase transition, we believe our results for the structure present indirect evidence for the importance of the dynamic clustering on the stabilization of the polar order for intermediate pullers systems. In order to verify the exact connection between these two quantities, we have to conduct a more detailed analysis on the dynamic clustering in bulk. We note that if we use a finer resolution of swimmers, we see the decrease in the exact value of the critical pipe di-

ameter D_c for the intermediate pullers: if we double the particle size, $\sigma = 12\Delta$, we obtain the critical diameter $D_c = 2\sigma$. (changes seems to be able to be seen only for the value of D_c). In other words, for intermediate pullers under strong confinement we require higher resolution to accurately resolve the flow around the particles. This resolution dependence can imply that smaller size clusters are enough for the polar order formation, like the ones with size corresponds to the peaks in $g(r)$. However, with the contemporary calculation power, the bulk simulation with such a finer resolution is too expensive to conduct with a realistic time and we cannot make a fair comparison between the results from the bulk simulation. Therefore, the discussion on the precise cluster size remains an open question. We confirmed the existence of the phase transition and the results are consistent between the two systems with different particle resolution. Our previous results [47] support this view on the importance of dynamic clustering. In ref.[47], we investigated whether or not the polar order seen in bulk can be explained only by the repetition of binary collisions. We found that this is the case, except for systems of intermediate pullers, which means that many particle interactions might be important in systems of intermediate pullers.

Finally, we have also considered pipes with diameters larger than 8σ . As the pipe size increases, we can expect that the dynamics approaches that seen in bulk systems. Indeed, for systems with $\alpha \neq 1$, we see in Fig. 3 that the order parameters in confinement agree very well with the bulk values. Thus, for these values of α , $D = 8\sigma$ seem to be big enough. Therefore, we have only considered larger diameters for $\alpha = 1$, to investigate whether a nonzero value of the polar order is recovered for a large enough pipe diameter. We considered diameters up to $D = 18\sigma$ but were not able to recover the bulk values in this case. Thus, the hypothesis stated in section III. B. is still not solved within the range of parameters considered in the present study. Although it is possible that the dynamics can change for even larger diameters, we will not discuss this problem any more, as it lies outside the scope of the present work.

D. Confinement shape dependency

The dynamics of fluids in pipes is known to depend on the shape of the cross section. Therefore, we have also investigated the effect of the shape dependency on the dynamics of the swimmers. So far, we have only considered dynamics in cylindrical pipes, with circular cross sections. Here, we consider pipes with a rectangular cross section. We refer to such confinement geometries as “ducts”. We considered two sizes of ducts, specified by a lateral size of 3σ and 8σ , respectively. Regarding the single-particle dynamics, the trajectories are qualitatively different from those in pipes for the case of pushers and neutral swimmers. Pullers will swim parallel to the duct axis, as they do in pipes. In ducts, regardless of the size, the tra-

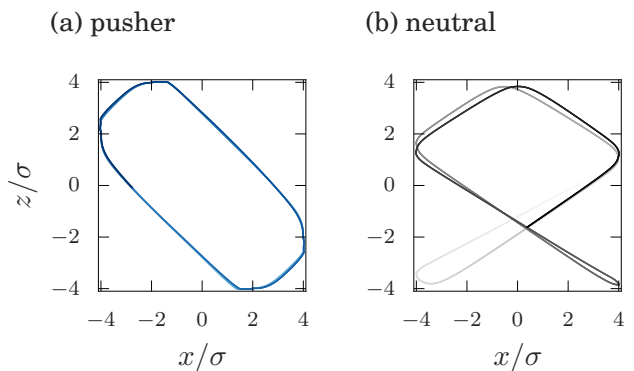


FIG. 9: The projection of the trajectories of a swimmer in duct onto the xz -plane. (a) Pusher with $\alpha = 1$. (b) Neutral swimmer. The lines represent the projections of the trajectories, with color intensity used to represent the time.

jectories of the pushers are spiral. Of course, reflecting the duct shape, the projections onto the xz -plane are no longer circular (Fig. 9). The neutral swimmer shows a similar spiral trajectory, but it has a strong dependency on the initial state and sometimes the trajectories can become more complicated (Fig. 9). Considering all the results for the single-particle system of pushers, we can conclude that the emergence of the circular closed orbits depends strongly on the curvature of the confining walls. Therefore, if we increase the diameter of the pipe continuously from 8σ , at some point we will find a critical value for pushers to lose their orbit-type characteristics. Such a detailed study is beyond our scope.

With regards to the many particle dynamics, we don’t see any big differences from those in pipes. Namely, the results are almost the same as those in bulk when the duct size is big enough, and the ordering seen for intermediate pullers collapses when the size is decreased. As a result, intriguingly, from the view point of the polar order of the many particle dispersion, the results are qualitatively the same between pipes and ducts. However, it is possible that we can observe unique dynamics in a skewed confinement.

IV. CONCLUSION

We investigated the polar order formation in pipes, conducting three-dimensional direct numerical simulation with fully resolved hydrodynamics. As a result of the investigation over a broad range of parameters, we confirmed that in most cases the dynamics of many particle systems in pipes match very well those in bulk. We have only observed considerable differences over a small range of parameters. We have presented an explanation for the emergence of wall effects by measuring the structural information. They are mostly due to the wall accumulating effects and the reduction in the degree of order in the vicinity of the walls. Also, we have studied the ef-

fects of the change in pipe size. We have clarified that for a specific range of the swimming parameter, the system undergoes an order/disorder phase transition when the size of the pipe shrinks. Considering the results of the structural analysis in bulk, we believe that this is due to the intrinsic clustering tendency of the swimmers. There seems to exist a minimum cluster size which is necessary to maintain the polar order of intermediate pullers. If we change the shape of the confinement, we found no qualitative differences, from the view point of the polar order. These results can be utilized to address the transport problem of microswimmers, however, further studies, like in winding pipes or in pipes with abrupt expansion/contraction are desired for realistic applications.

V. ACKNOWLEDGMENTS

We thank H. Ito for enlightening discussions. This work was supported by the Japan Society for the Promotion of Science (JSPS) KAKENHI Grant No. 26247069 and also by a Grant-in-Aid for Scientific Research on Innovative Areas Dynamical ordering of biomolecular systems for creation of integrated functions (No. 16H00765) from the Ministry of Education, Culture, Sports, Science, and Technology of Japan. We also acknowledge the supporting program for interaction-based initiative team studies (SPIRITS) of Kyoto University.

-
- [1] M. C. Marchetti, J. F. Joanny, S. Ramaswamy, T. B. Liverpool, J. Prost, M. Rao, and R. A. Simha, *Rev. Mod. Phys.* **85**, 1143 (2013).
 - [2] S. C. Takatori, W. Yan, and J. F. Brady, *Phys. Rev. Lett.* **113**, 028103 (2014).
 - [3] A. P. Solon, Y. Fily, A. Baskaran, M. E. Cates, Y. Kafri, M. Kardar, and J. Tailleur, *Nat. Phys.* **11**, 1 (2015).
 - [4] É. Fodor, C. Nardini, M. E. Cates, J. Tailleur, P. Visco, and F. van Wijland, *Phys. Rev. Lett.* **117**, 038103 (2016).
 - [5] N. Nikola, A. P. Solon, Y. Kafri, M. Kardar, J. Tailleur, and R. Voituriez, *Phys. Rev. Lett.* **117**, 098001 (2016).
 - [6] A. Zöttl and H. Stark, *J. Phys. Condens. Matter* **28**, 253001 (2016).
 - [7] C. Bechinger, R. Di Leonardo, H. Löwen, C. Reichhardt, G. Volpe, and G. Volpe, *Rev. Mod. Phys.* **88**, 045006 (2016).
 - [8] T. Speck, *EPL (Europhysics Lett.)* **114**, 30006 (2016).
 - [9] J. Blaschke, M. Maurer, K. Menon, A. Zöttl, and H. Stark, *Soft Matter* (2016).
 - [10] R. G. Winkler, *Eur. Phys. J. Spec. Top.* **225**, 2079 (2016).
 - [11] E. Lauga and T. R. Powers, *Rep. Prog. Phys.* **72**, 96601 (2009).
 - [12] J. Elgeti, R. G. Winkler, and G. Gompper, *Rep. Prog. Phys.* **78**, 056601 (2015).
 - [13] W. F. Paxton, K. C. Kistler, C. C. Olmeda, A. Sen, S. K. St. Angelo, Y. Cao, T. E. Mallouk, P. E. Lammert, and V. H. Crespi, *J. Am. Chem. Soc.* **126**, 13424 (2004).
 - [14] W. F. Paxton, S. Sundararajan, T. E. Mallouk, and A. Sen, *Angew. Chemie Int. Ed.* **45**, 5420 (2006).
 - [15] M. N. Popescu, W. E. Usual, and S. Dietrich, *Eur. Phys. J. Spec. Top.* **225**, 2189 (2016).
 - [16] K. Kroy, D. Chakraborty, and F. Cichos, *Eur. Phys. J. Spec. Top.* **225**, 2207 (2016).
 - [17] R. Seemann, J.-B. Fleury, and C. C. Maass, *Eur. Phys. J. Spec. Top.* **225**, 2227 (2016).
 - [18] Z. Izri, M. N. Van Der Linden, S. Michelin, and O. Dautot, *Phys. Rev. Lett.* **113** (2014).
 - [19] E. Lushi, H. Wioland, and R. E. Goldstein, *Proc. Natl. Acad. Sci.* **111**, 9733 (2014).
 - [20] A. A. Evans, T. Ishikawa, T. Yamaguchi, and E. Lauga, *Phys. Fluids* **23**, 111702 (2011).
 - [21] F. Alarcón and I. Pagonabarraga, *J. Mol. Liq.* **185**, 56 (2013).
 - [22] N. Oyama, J. J. Molina, and R. Yamamoto, *Phys. Rev. E* **93**, 043114 (2016).
 - [23] J. Elgeti and G. Gompper, *Eur. Phys. J. Spec. Top.* **225**, 2333 (2016).
 - [24] A. Wysocki, J. Elgeti, and G. Gompper, *Phys. Rev. E* **91** (2015).
 - [25] S. E. Spagnolie, G. R. Moreno-Flores, D. Bartolo, and E. Lauga, *Soft Matter* **11**, 3396 (2015).
 - [26] S. Das, A. Garg, A. I. Campbell, J. Howse, A. Sen, D. Velegol, R. Golestanian, and S. J. Ebbens, *Nat. Commun.* **6**, 8999 (2015).
 - [27] L. Zhu, E. Lauga, and L. Brandt, *J. Fluid Mech.* **726**, 285 (2013).
 - [28] G.-J. Li and A. M. Ardekani, *Phys. Rev. E* **90**, 013010 (2014).
 - [29] A. Zöttl and H. Stark, *Phys. Rev. Lett.* **112**, 118101 (2014).
 - [30] K. Ishimoto and E. A. Gaffney, *Phys. Rev. E* **88**, 062702 (2013).
 - [31] M. Theers, E. Westphal, G. Gompper, and R. G. Winkler, *Soft Matter* **12**, 7372 (2016).
 - [32] S. E. Spagnolie and E. Lauga, *J. Fluid Mech.* **700**, 105 (2012).
 - [33] P. Maggaretti and H. Stark, *J. Chem. Phys.* **146**, 174901 (2017).
 - [34] J. de Graaf, A. J. T. M. Mathijssen, M. Fabritius, H. Menke, C. Holm, and T. N. Shendruk, *Soft Matter* **12**, 4704 (2016).
 - [35] M. N. Popescu, S. Dietrich, and G. Oshanin, *J. Chem. Phys.* **130**, 194702 (2009).
 - [36] J.-T. Kuhr, J. Blaschke, F. Rühle, and H. Stark, *arXiv:1706.04527* (2017).
 - [37] H. Stark, *Eur. Phys. J. Spec. Top.* **225**, 2369 (2016).
 - [38] A. Zöttl and H. Stark, *Phys. Rev. Lett.* **108**, 218104 (2012).
 - [39] L. Jibuti, L. Qi, C. Misbah, W. Zimmermann, S. Rafai, and P. Peyla, *Phys. Rev. E* **90**, 063019 (2014).
 - [40] M. J. Lighthill, *Commun. Pure Appl. Math.* **5**, 109 (1952).
 - [41] J. R. Blake, *J. Fluid Mech.* **46**, 199 (1971).
 - [42] T. Ishikawa, M. P. Simmonds, and T. J. Pedley, *J. Fluid Mech.* **568**, 119 (2006).
 - [43] Y. Nakayama and R. Yamamoto, *Phys. Rev. E* **71**, 036707 (2005).
 - [44] K. Kim, Y. Nakayama, and R. Yamamoto, *Phys. Rev.*

- Lett. **96**, 1 (2006).
- [45] Y. Nakayama, K. Kim, and R. Yamamoto, Eur. Phys. J. E **26**, 361 (2008).
 - [46] J. J. Molina, Y. Nakayama, and R. Yamamoto, Soft Matter **9**, 4923 (2013).
 - [47] N. Oyama, J. J. Molina, and R. Yamamoto, arXiv:1606.03839v1 (2016).
 - [48] J. Elgeti and G. Gompper, EPL (Europhysics Lett. **101**, 48003 (2013).
 - [49] A. Costanzo, J. Elgeti, T. Auth, G. Gompper, and M. Ripoll, EPL (Europhysics Lett. **107**, 36003 (2014).
 - [50] W. B. Russel, D. A. Saville, and W. R. Schowalter, *Colloidal Dispersions* (1989).